Macromolecules

Open Access

pubs.acs.org/Macromolecules

Article

How Do Polymers Stretch in Capillary-Driven Extensional Flows?

Vincenzo Calabrese,* Amy Q. Shen, and Simon J. Haward*

Cite This: *Macromolecules* 2024, 57, 9668−9676

Read Online

ACCESS | Metrics & More | Article Recommendations | Supporting Information

ABSTRACT: Measurements of the capillary-driven thinning and breakup of fluid filaments are widely used to extract the extensional rheological properties of complex materials. For viscoelastic fluids, such as polymer solutions, the longest relaxation time of the polymer is inferred from the decay rate of the filament diameter in the elastocapillary thinning regime. However, this determination relies on assumptions from constitutive models that are challenging to validate experimentally. By comparing the response of fluids in capillary thinning with that in a microfluidic extensional flow (in which the polymeric dynamics can be readily assessed), we show experimentally that these assumptions are likely only valid for highly extensible polymers but do not hold in general. For polymers with relatively low extensibility, such as polyelectrolytes in salt-free media, the conventional extrapolation of the longest relaxation time from capillary thinning techniques leads to a significant underestimation. We explain this discrepancy by considering the macromolecular dynamics occurring in the initial Newtonian-like thinning regime prior to the onset of elastocapillarity.

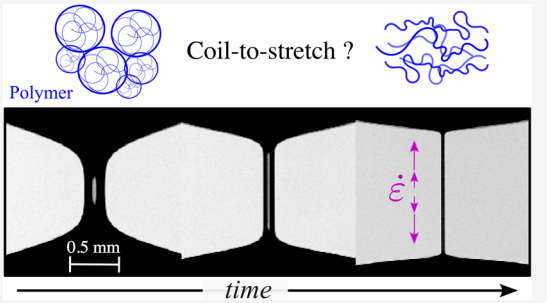

INTRODUCTION

Measuring the diameter D as a function of time t at the midpoint of a fluid filament as it thins under the action of capillarity has become a common method for estimating the extensional rheological properties of polymeric fluids. There are many methods for initiating the capillary-driven thinning of a liquid bridge, the subsequent dynamics of which can all be analyzed in a roughly similar way to obtain rheometric data.[1−11] We focus on a technique termed the slow retraction method (SRM),[2] in which a fluid sample is loaded between coaxial circular plates initially separated vertically by a small distance (∼1 mm). The bottom plate is gradually displaced vertically downward until the liquid bridge between the plates (now at a critical diameter, $D = D_0$) becomes unstable to capillary forces and begins to break up. For a Newtonian fluid in the absence of inertia, the liquid bridge attains an hourglass shape and undergoes viscocapillary (VC) thinning, during which the filament diameter decays linearly with time at a rate that depends on the surface tension σ and the shear viscosity η (as shown by Papageorgiou, see Figure 1).[12,13] For a polymeric fluid, the (inertialess) thinning of the liquid bridge at short times is Newtonian-like (Figure 1) and commonly associated with the initially coiled state of the polymer. Importantly, in the VC regime, the extension rate in the fluid neck (estimated by $\dot{\varepsilon}(t) = -[2/D(t)]\mathrm{d}D(t)/\mathrm{d}(t)$) increases monotonically with time.

According to the prediction of the Oldroyd-B constitutive model, which considers a polymer as being infinitely extensible, as $\dot{\varepsilon}$ increases beyond a critical value $\dot{\varepsilon}_c$, polymers in the fluid filament begin to deform from their equilibrium coils and accumulate strain. As the polymer stretches, the elastic stress

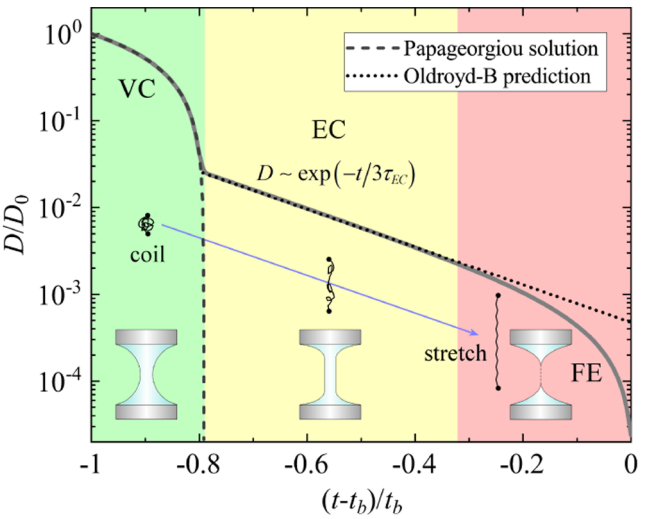

Figure 1. A schematic representation of a typical capillary-thinning experiment (e.g., SRM) performed with a viscoelastic fluid sample. The filament diameter D is normalized by the critical diameter D_0, at which the capillary-driven self-thinning of the filament commences. The time t is normalized by the breakup time t_b. See text for a detailed description.

Received: July 11, 2024
Revised: August 22, 2024
Accepted: September 18, 2024
Published: October 10, 2024

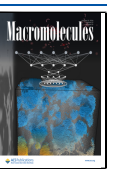

grows and begins to dominate over the viscous stress. Consequently, the thinning behavior of the filament diverges from the Newtonian case, leading to the onset of an elastocapillary (EC) thinning regime (Figure 1).[1,14−16] Through the EC regime, the filament develops a slender columnar shape, the diameter of which decays exponentially in time with the consequence that $\dot{\varepsilon}$ becomes constant with a value $\dot{\varepsilon}_{EC}$.[17,18] However, there is no control over the value of $\dot{\varepsilon}_{EC}$, which is self-selected by the fluid via the force balance. Fitting the exponential decay in the EC regime with the form

$$D \sim \exp(-t/3\tau_{EC}) \quad (1)$$

is a standard procedure used to extract a characteristic time constant for the fluid (here denoted as τ_{EC}). This time constant is often considered to be a fundamental material property, commonly described as the longest relaxation time (τ) of the polymer.[10] It can be shown that $\dot{\varepsilon}_{EC}\tau_{EC} = 2/3$,[19] thus it is assumed that the Weissenberg number in the EC regime $Wi_{EC} = \dot{\varepsilon}_{EC}\tau = 2/3$ (i.e., $Wi_{EC} > \dot{\varepsilon}_c\tau = 0.5$), and hence, that polymers will become stretched.[20−23]

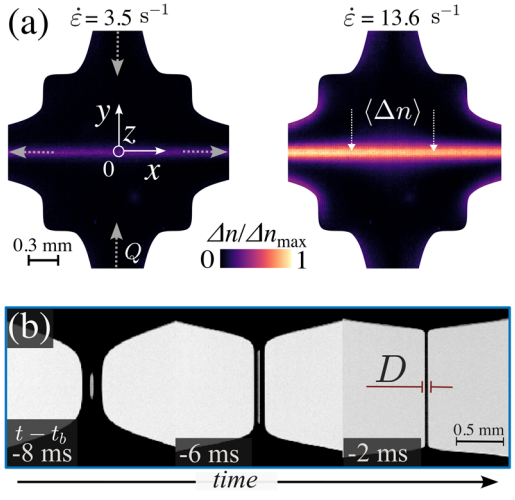

Figure 2. (a) Birefringence Δn (normalized by its maximum value, Δn_{max}) in a λ-DNA solution at $c = 1.1c^*$, flowing in a microfluidic OSCER geometry at two well-defined extension rates. The flow in each arm is driven by a syringe pump operating at a controlled volumetric rate Q. The flow scheme and coordinate system are indicated in the left-hand image. The location where the time-averaged intensity of the birefringent strand, $\langle\Delta n\rangle$, is retrieved is indicated in the right-hand image. The OSCER generates a planar extensional flow that is shear-free around the stagnation point $x = y = 0$ mm, the extension being along the x direction. (b) Snapshots at different moments during an SRM experiment with the same λ-DNA solution used in part (a).

For the Oldroyd-B model, which considers a polymer as infinitely extensible, the EC regime is predicted to persist indefinitely. However, for real polymeric fluids, the filament thinning eventually becomes super exponential and the filament undergoes pinch-off at time $t = t_b$ (Figure 1). The finite t_b can be predicted by including finite extensibility in the constitutive model, hence the labeling of this terminal "FE" regime.[1,15,24] The finitely extensible nonlinear elastic (FENE) dumbbell model predicts that, as polymers approach full extension, they begin to behave as rigid rods. In the FE regime, the fluid exhibits Newtonian-like behavior, with the filament thinning linearly in time, similar to the VC regime but with a higher extensional viscosity due to the polymers being stretched.[25−27]

The Oldroyd-B and FENE models predict an intimate connection between the macromolecular and the filament thinning dynamics, which was largely borne out by early capillary thinning measurements performed on solutions of highly flexible polymers with well-defined molecular parameters.[1,28] However, the direct assessment of polymer dynamics during capillary thinning remains untested due to considerable experimental difficulties. This may explain why predictions from the Oldroyd-B and FENE models have been broadly applied to interpret capillary thinning data obtained from almost any type of polymer in any solvent.[29−41]

Of particular relevance, we refer to solutions of fluorescently labeled DNA (considered as a model polymer for molecular rheology),[42] the dynamics of which have been directly observed under high fluid strains in steady extensional flows in cross-slot devices at precisely controlled values of $\dot{\varepsilon}$.[43,44] Such experiments provide a clear and unambiguous value for the longest relaxation time $\tau = 0.5/\dot{\varepsilon}_c \sim O$ (s), where $\dot{\varepsilon}_c$ is the extension rate beyond which the DNA molecules are seen to accumulate strain.[23,43−45] However, capillary thinning experiments on similar fluids show weakly pronounced EC regimes suggestive of characteristic times $\tau_{EC} \sim O$ (ms),[46] i.e., $\tau_{EC} \ll \tau$, an apparent inconsistency that strongly motivated the current work.

In this article, we provide insight into the polymer dynamics occurring during the capillary thinning of polymeric fluids, highlighting the strengths and limitations of filament thinning techniques for extensional rheometry. We provide a generalized perspective by analyzing a wide variety of polymers with different extensibility $L = l_c/\sqrt{\langle R^2\rangle}$, where l_c is the contour length and $\langle R^2\rangle$ is the mean-squared end-to-end length of the polymer at rest. For each polymeric solution, we perform birefringence measurements in an optimized form of the microfluidic cross-slot geometry (e.g., see Figure 2a)[47,48] to determine a value of τ associated with the longest time scale at which polymer chains exhibit anisotropy. We also examine the response in an SRM experiment (e.g., Figure 2b) to obtain a value for τ_{EC}. Our findings reveal a clear correlation between the ratio τ_{EC}/τ and L, showing $\tau_{EC} \approx \tau$ for large extensibility but a strong decrease in τ_{EC}/τ as L becomes small. By integrating the strain rates measured over time during capillary thinning experiments, we show that for high L, the estimates of macromolecular strain are in line with the predictions of the Oldroyd-B model. However, when considering polymers with lower L, a considerable extension may occur even before the EC regime initiates, a dynamic that is not captured by Oldroyd-B and which renders eq 1 inadequate for the extrapolation of the longest relaxation time of the polymer.

RESULTS AND DISCUSSION

Prior to the analysis of a wide spectrum of polymeric species, we begin the presentation of our results by considering two distinct but model polymeric systems, namely a relatively stiff λ-DNA with $L \approx 12$ in a viscous buffer solution and a more extensible polystyrene (PS) with $L \approx 117$ in a viscous θ-solvent.[42]

λ-DNA. Figure 2 displays exemplary results for a λ-DNA solution in a viscous buffer solution (Tris-EDTA, 5 mM NaCl,

https://doi.org/10.1021/acs.macromol.4c01604
Macromolecules 2024, 57, 9668−9676

and sucrose with viscosity $\eta_s = 4.3$ mPa s) in an optimized-shape cross-slot extensional rheometer (OSCER, Figure 2a) and during an SRM experiment (Figure 2b). The λ-DNA has extensibility $L \approx 12$ and is prepared at a concentration $c = 1.1c^*$, where $c^* = 40$ μg/mL is the estimated overlap concentration[49] (Table S1). Figure 2a shows the birefringence Δn at two distinct extension rates $\dot{\varepsilon} \approx 0.2Q/(W^2H)$, where Q is the volumetric flow rate and H and W are the height and width of the channel, respectively.[47] Above a critical extension rate, $\dot{\varepsilon}_c$, the polymer starts to unravel and a birefringent strand appears along the x-axis of the device. With increasing $\dot{\varepsilon}$, the intensity of the birefringent strand increases, indicating pronounced DNA stretching. In the SRM experiment (Figure 2b), we utilize high-speed imaging to monitor the filament as it undergoes self-thinning over time t until it reaches pinch-off at time $t = t_b$. For $t - t_b > -8$ ms, the filament develops a cylindrical shape, characteristic of the EC regime encountered for polymer solutions.

From the OSCER experiment, we retrieve the time-averaged intensity of the birefringent strand, $\langle \Delta n \rangle$ (i.e., at $y = 0$ mm for $-1.5\ \text{W} \lesssim x \lesssim 1.5$ W, see Figure 2a) as a function of $\dot{\varepsilon}$, as shown normalized by the polymer mass fraction (ϕ) in Figure 3a. Linear extrapolation of the birefringence data for small $\dot{\varepsilon}$ (red line, inset Figure 3a) provides a precise value of $\dot{\varepsilon}_c = 1.2\ \text{s}^{-1}$ for the onset of orientation of the polymer chains. Since at the onset of birefringence we expect the Weissenberg number $Wi = \dot{\varepsilon}\tau \approx 0.5$,[23,43−45] the relaxation time can be estimated as $\tau \approx 0.5/\dot{\varepsilon}_c$; hence, $\tau = 0.42$ s. Previous experiments, conducted using various techniques (both bulk shear rheometry and single molecule imaging),[45,49−53] are consistent with our measurement of τ. Accounting for the effects of concentration and solvent viscosity, single-molecule imaging experiments[45,49−51] suggest $\tau \approx 0.5$ s, while an estimate of the Rouse relaxation time based on an experimental intrinsic viscosity measurement gives $\tau \approx 0.3$ s,[52] in close agreement with $\tau = 0.42$ s obtained from our microfluidic experiment.

The value of τ retrieved from the microfluidic experiment suggests an elastocapillary number in the SRM experiment $Ec = 2\tau\sigma/\eta_s D_p \gg 1$, where $D_p = 6$ mm is the diameter of the end-plates. This suggests that the elastic stress from the polymer should be sufficient to dominate over the viscous stress of the solvent, provided that the polymer concentration is sufficiently high.[16] From the balance between the viscous stresses of the solvent and the elastic stress of fully stretched polymer, Clasen et al.,[16] defined the minimum polymer concentration necessary for a significant elastic contribution to emerge in a capillary thinning experiment as,

$$c_{\min} = \frac{3\text{Mw}\eta_s}{2RT\tau_0 L^2}. \tag{2}$$

In eq 2, Mw is the molecular weight, R is the gas constant, T is the temperature, and τ_0 is the longest polymer relaxation time of the dilute polymer solution. For the λ-DNA solution ($\eta_s = 4.3$ mPa s) with $0.2 \lesssim \tau_0 \lesssim 0.4$ s,[45,50−52] we estimate $c_{\min} \approx 1.8$ μg/mL. The concentration of the tested λ-DNA solution is therefore $c > 20 \times c_{\min}$. Despite the relatively large values for both Ec and c, the λ-DNA solution shows a narrow EC regime where D decreases exponentially over time ($-8 \lesssim t - t_b \lesssim -3$ ms, Figure 3b). The presence of the EC regime is also clear from the plateau-like region in $\dot{\varepsilon}$ vs $t - t_b$ (Figure 3c). By fitting eq 1 to the EC region, we retrieve $\tau_{EC} = 1.1$ ms, a value much smaller than τ obtained from the birefringence experiment ($\tau_{EC} \approx \tau/380$). Consequently, the steady value of $\dot{\varepsilon}_{EC}$ sets $Wi_{EC} = \dot{\varepsilon}_{EC}\tau \approx 250$, in stark contrast to the value of $Wi_{EC} = 2/3$ predicted by the Oldroyd-B and FENE models.

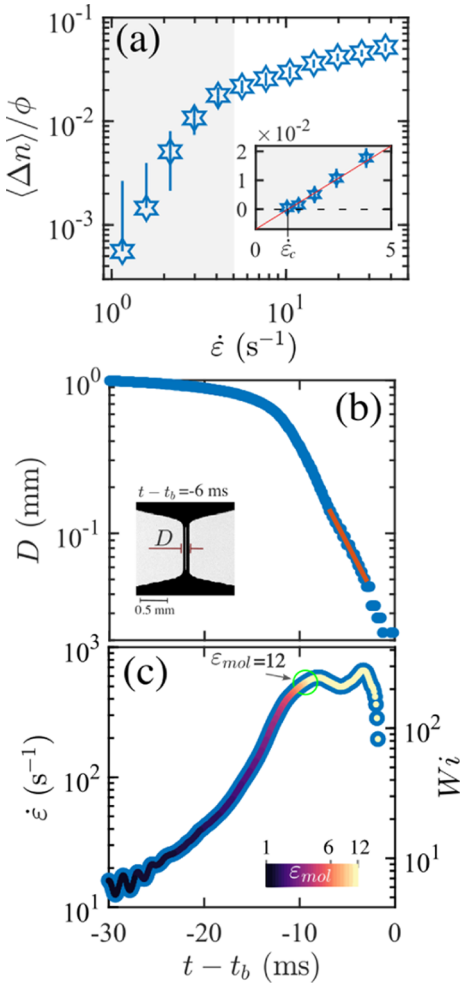

Figure 3. Results from (a) microfluidic and (b, c) SRM experiment for a λ-DNA solution at $c = 1.1c^*$. (a) The time-averaged intensity of the birefringent strand $\langle \Delta n \rangle$, normalized by the polymer mass fraction ϕ, as a function of the extension rate $\dot{\varepsilon}$. The inset shows the linear-linear plot of $\langle \Delta n \rangle/\phi$ vs $\dot{\varepsilon}$ with the linear fitting at $\langle \Delta n \rangle/\phi \to 0$ used to estimate the extension rate at the onset of birefringence ($\dot{\varepsilon}_c$), and the relaxation time $\tau = 0.5/\dot{\varepsilon}_c$. (b) Filament diameter D as a function of time $t - t_b$. The line is the fit to eq 1. (c) The extension rate at the neck of the filament ($\dot{\varepsilon}(t) = -[2/D(t)]\text{d}D(t)/\text{d}(t)$) and the respective $Wi = \dot{\varepsilon}\tau$ as a function of time $t - t_b$. The color scale indicates the accumulated macromolecular strain, ε_{mol}. The arrow in (c) indicates the location $\varepsilon_{\text{mol}} = 12$ where the complete stretch of the chains is estimated.

In general, if coiled macromolecules are exposed to a persistent extensional flow with $Wi = \dot{\varepsilon}\tau \gtrsim 0.5$, then macromolecular strain should accumulate over time. We roughly estimate, similarly to ref. 23, the accumulated macromolecular strain in the SRM experiment as $\varepsilon_{\text{mol}}(t) = \exp\left(\int_{-t_b}^{t} (\dot{\varepsilon} - \dot{\varepsilon}_c)\text{d}t\right)$ for $Wi \geq 0.5$. We expect (assuming affine deformation of the polymer for any $Wi \geq 0.5$) that the λ-DNA reaches a fully stretched state when $\varepsilon_{\text{mol}} \gtrsim L \approx 12$. Based on our estimate (shown by the color-coded data points in Figure 3c), the value

https://doi.org/10.1021/acs.macromol.4c01604
Macromolecules 2024, 57, 9668−9676

of $\varepsilon_{mol} = 12$ is reached at $t - t_b \approx -10$ ms, suggesting that the polymer is likely to be highly stretched even before the onset of the EC regime, a scenario that is not predicted by the Oldroyd-B model. Single- molecule imaging of λ-DNA during capillary thinning in a flow-focusing microfluidic device has also shown that the DNA molecules become highly aligned during the Newtonian-like thinning of the fluid neck, with the absence of a clear EC regime.[54]

Following Campo-Deaño and Clasen,[2] we estimate the low concentration limit (c_{low}), above which the onset of polymer stretching coincides with the onset of the EC regime (as predicted by the Oldroyd-B model):

$$c_{low} = \frac{1}{2.46}\frac{Mw}{RT}\left(\frac{\sigma^2\rho}{\tau_0^2}\right)^{1/3}L^{-3/2} \quad (3)$$

where ρ is the fluid density. We compute $c_{low} \approx 12c^* \approx 470$ μg/mL, indicating that our experiment at $1.1c^*$ is in the regime $c_{min} < c < c_{low}$. The implicit assumption in c_{low} is the diluteness of the polymer chains. However, at $c_{low} \approx 12c^*$, λ-DNA is an highly entangled state.[49,55] For completeness, we performed a second SRM experiment for a λ-DNA solution at a concentration $c > c_{low}$ (i.e., $c_{low} = 16.5c^* = 660$ μg/mL), yielding $\tau_{EC} \approx 4$ ms (Figure S1). Given the required volume, it is unfeasible for us to perform the comparative microfluidic experiment to retrieve τ at $c = 660$ μg/mL. However, we can compare $\tau_{EC} \approx 4$ ms with $\tau \approx 22.5$ s obtained from single-molecule experiments ($\tau \approx 75\tau_0$).[49,55] Despite operating at $c > c_{low}$, we still find a strong inconsistency between the two time scales with $\tau_{EC}/\tau \sim O(10^{-4})$.

Polystyrene. We compare our analysis for the λ-DNA with a significantly more extensible polymer that aligns more closely with the assumptions of the Oldroyd-B model, namely PS with molecular weight Mw = 7 MDa in a θ-solvent (dioctyl phthalate, DOP) and a resulting $L \approx 117$. The dilute PS solution ($c = 0.025c^* > c_{low} > c_{min}$, $Ec \approx 1$) shows an onset of birefringence at $\dot{\varepsilon}_c = 76\ s^{-1}$ (Figure 4a), from which a relaxation time $\tau = 6.5$ ms is estimated. In the SRM experiment (Figure 4b), the PS solution shows a clear EC thinning regime, yielding $\tau_{EC} = 10$ ms (eq 1), in reasonable agreement with the value $\tau = 6.5$ ms obtained from the birefringence experiment. As such, the steady-state region of $\dot{\varepsilon}_{EC}$ yields $Wi_{EC} \approx 0.5$, close to the $Wi_{EC} = 2/3$ expected from the Oldroyd-B model (Figure 4c). An estimate of the macromolecular strain in this case (see the color-coded data points in Figure 4c) indicates that the transition into the EC regime (i.e., beyond the peak in $\dot{\varepsilon}$ at $t - t_b \approx -40$ ms) roughly coincides with the initial unraveling of the polymers (i.e., $\varepsilon_{mol} > 1$) and that maximum extension is approached (i.e., $\varepsilon_{mol} \to L$) toward the end of the experiment at $t = t_b$. In this case, our roughly estimated macromolecular dynamics are in broad agreement with the Oldroyd-B model. Accordingly, we observe consistency between τ_{EC} and the longest relaxation time τ.[2]

From Flexible to Rigid Polymers. While both PS and λ-DNA share the presence of the EC regime at the macroscopic fluid level, the underlying polymer dynamics occurring during the EC regime are distinct. We use the ratio τ_{EC}/τ to capture the polymer dynamics occurring in capillary thinning for polymers with a wide range of extensibility, L. For stiffer polymers, we use hyaluronic acid (HA) and carboxymethyl cellulose (CMC) in deionized water, along with monodisperse λ-DNA (discussed above) and polydisperse calf thymus DNA

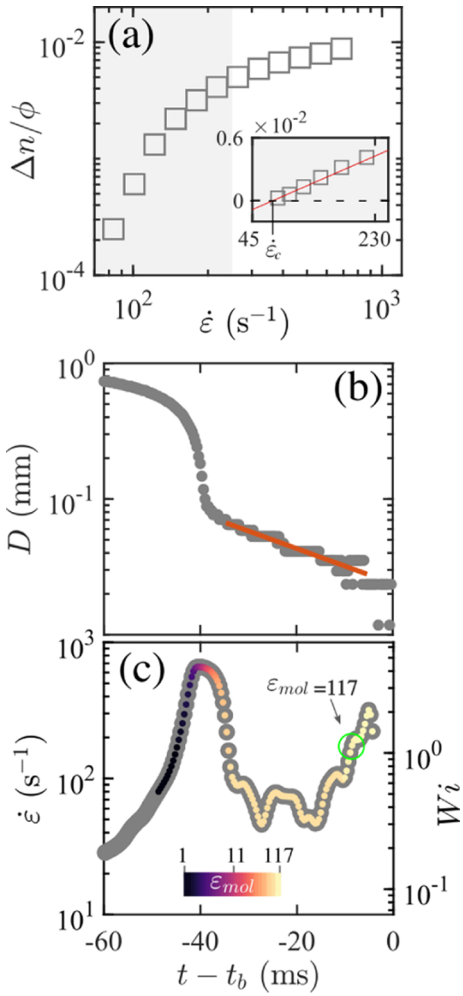

Figure 4. Results from (a) microfluidic and (b, c) SRM experiments for a PS solution (Mw = 7 MDa) at $c = 0.025c^*$. (a) Time-averaged intensity of the birefringent strand $\langle\Delta n\rangle$, normalized by the mass fraction ϕ, as a function of the extension rate $\dot{\varepsilon}$. The inset shows the lin-lin plot of $\langle\Delta n\rangle/\phi$ vs $\dot{\varepsilon}$ with the linear fitting at $\langle\Delta n\rangle/\phi \to 0$ used to estimate the extension rate at the onset of birefringence ($\dot{\varepsilon}_c$) and the relaxation time $\tau = 0.5/\dot{\varepsilon}_c$. (b) Filament diameter D as a function of time $t = t_b$. The line is the fitting to eq 1. (c) Extension rate at the neck of the filament ($\dot{\varepsilon}(t) = -[2/D(t)]\mathrm{d}D(t)/\mathrm{d}(t)$) and the respective $Wi = \dot{\varepsilon}\tau$ as a function of time $t = t_b$. The color scale indicates the accumulated macromolecular strain, ε_{mol}. The arrow in (c) indicates the location $\varepsilon_{mol} = 117$ where the complete stretch of the chains is estimated.

(ct-DNA) with an average contour length comparable to that of the λ-DNA. For more flexible polymers, we use PS in DOP, poly(ethylene oxide) (PEO) in aqueous polyethylene glycol (PEG, Mw = 8 kDa) solution, and hyaluronic acid in a 1.5 M NaCl aqueous solution (HA_{NaCl}), all with a range of Mw. Polymer concentrations, typically between the dilute and semidilute regimes, are chosen to be as low as possible but still sufficient to probe the EC region in the SRM[16] experiment and have detectable birefringence in the microfluidic OSCER device (see Supporting Information for detailed specifications of the tested polymer samples). Note that we tested several fluids by SRM using end plates of various diameter, with no systematic variation in the obtained values of τ_{EC} (data shown in Supporting Information).[10]

https://doi.org/10.1021/acs.macromol.4c01604
Macromolecules 2024, 57, 9668−9676

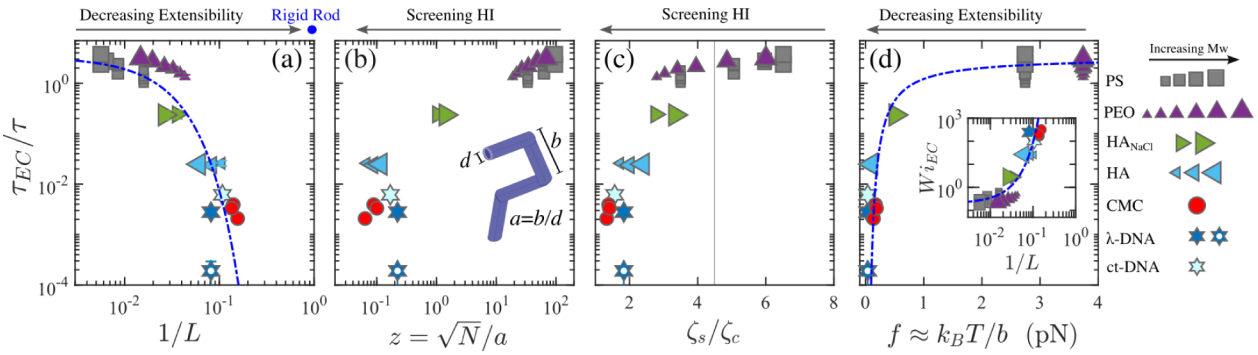

Figure 5. Ratio τ_{EC}/τ as a function of (a) $1/L$, (b) $z = \sqrt{N}/a$, (c) ζ_s/ζ_c, and (d) $f \approx k_BT/b$ for different polymer solutions. Insert in (d) shows the Weissenberg number in the EC regime Wi_{EC} as a function of $1/L$. The dash-dotted lines, given as reference functions, are (a) $\tau_{EC}/\tau = 3.3\exp(55/(1-L))$, (d) $\tau_{EC}/\tau = 3.3\exp(-1/f)$ and (d, insert) $Wi_{EC} = 0.2\exp(55/(L-1))$. For a given polymer, increasing Mw is depicted by an increasing symbol size. For the PS and CMC, multiple data points indicate different concentrations. The higher concentration of λ-DNA ($c = 660\ \mu g/mL$), where τ_{EC} is compared with τ from single-molecule experiments[49,55] is labeled by an additional white dot in the symbol.

In Figure 5a, we plot the ratio τ_{EC}/τ as a function of $1/L$. For the most flexible PS and PEO polymers with $L \gtrsim 30$, we observe that $\tau_{EC}/\tau \sim O(1)$. We note that this result holds despite the widely different volatility of the respective solvents.[56] For more rigid polymers with $L < 30$, τ_{EC}/τ decreases significantly below unity. Regardless of the concentration, for the stiff λ-DNA (below and above c_{low}) and CMC (multiple red circles in Figure 5), $\tau_{EC}/\tau \ll 1$. At least qualitatively, it is clear that as $1/L$ increases, τ_{EC}/τ decreases. Possible reasons for the extent of data scatter could be linked to differences in sample polydispersity,[57] the difficulty in estimating cL, and the inherent molecular differences between the tested polymers. Nonetheless, our results are in line with the recent numerical simulations of isolated FENE chains by Zinelis et al., showing that for relatively stiff chains, τ_{EC} significantly underestimates the longest relaxation time.[58]

We interpret the trend of τ_{EC}/τ as a function of polymer extensibility as follows: In the birefringence experiment, we measure the longest relaxation time τ, associated with the time scale $(0.5/\dot{\varepsilon}_c)$ at which the orientation of the polymer chains occurs.[23] On the other hand, the capillary thinning experiment relies on the stretching polymer to induce sufficient elastic stress in order to dominate the stress from the solvent and initiate an EC thinning regime.[16] We may consider τ_{EC} as a time scale associated with the onset of *measurable* elastic stresses (by which we mean sufficient to cause a deviation from Newtonian-like thinning).[16,24] Evidently, τ and τ_{EC} are not, in general, the same.

For highly flexible polymers, such as PS and PEO, $\tau_{EC}/\tau \sim O(1)$ (Figure 5), indicating that the time scale of chain orientation corresponds to the time scale at which elastic stresses become detectable in a capillary thinning experiment. Note that for flexible polymer solutions, τ_{EC} cannot be significantly greater than τ as the polymer must orient and stretch for the elastic stress to develop.

With decreasing polymer extensibility, τ_{EC} decreases relative to τ. This suggests that chain orientation occurs on a longer time scale than that required for observing elastic effects in the capillary thinning experiment. It is instructive to consider the limiting case of rigid rod-like polymers ($L = 1$), which orient in flow at an extension rate $\dot{\varepsilon}_c$ sufficient to overcome rotational diffusion and thus have finite $\tau > 0$.[59−62] However, since rigid rod-like polymers have negligible entropic elasticity,[63] we expect $\tau_{EC} \to 0$ and the total absence of the EC regime (see refs.[64−66]). Therefore, we expect two natural asymptotes in the plot of τ_{EC}/τ vs $1/L$: $\tau_{EC}/\tau \to \sim 1$ as $1/L \to 0$, and $\tau_{EC}/\tau \to 0$ as $1/L \to 1$. This is roughly captured by the empirically determined function $\tau_{EC}/\tau = 3.3\exp(55/(1-L))$ (dash-dotted line in Figure 5a).

In Figure 5b, we plot the ratio τ_{EC}/τ as a function of a chain interaction parameter $z = \sqrt{N}/a$ (where N is the number and $a = b/d$ is the aspect ratio of each Kuhn segment in the polymer chain, with b and d as the length and thickness, respectively). For large Mw polymers with relatively small Kuhn segments, $z > 1$ indicates strong intramolecular hydrodynamic interactions (HI).[42] The relatively rigid λ-DNA and the relatively flexible PS (Mw = 7 MDa) previously described have estimated values of $z = 0.45$ and $z = 60$, respectively. This indicates that the λ-DNA coil adopts a free-draining configuration with screened HI that keep the polymer segments hydrodynamically unshielded.[42] On the contrary, the PS with $z \gg 1$ forms a nonfree-draining coil with hydrodynamically shielded polymer segments.

The ratio of the hydrodynamic drag between the stretched (ζ_s) and coiled (ζ_c) conformations of a polymer, estimated as $\zeta_s/\zeta_c \approx (N^2a)^{1/5}/\ln(Na)$, gauges the importance of HI to the stretching dynamics.[42,43,67] Based on experiments and simulations, $\zeta_s/\zeta_c \approx 4.5$ sets the threshold value above which HI become dominant and the polymer segments are hydrodynamically shielded. The plot of τ_{EC}/τ as a function of ζ_s/ζ_c shows that the plateau $\tau_{EC}/\tau \sim O(1)$ is reached for $\zeta_s/\zeta_c \gtrsim 4$ (Figure 5c). Based on the analysis of the parameters z and ζ_s/ζ_c, we hypothesize that for stiffer polymers with screened HI (i.e., $z < 1$ and $\zeta_s/\zeta_c \lesssim 4.5$) chain orientation readily occurs even before the EC sets in, resulting in $\tau_{EC} < \tau$. Additionally, stiffer polymers exert less stress on the flow. This is evidenced by computing the chain tension above which the polymer behaves as a nonlinear spring, $f \approx k_BT/b$, where k_B is the Boltzmann constant and T is the temperature (Figure 5d).[63] For the more flexible chains (PS and PEO) with significant HI, this force is several pico Newtons per chain, but for the stiffer chains (e.g., CMC and DNA), f is extremely low.

We suggest that for sufficient concentrations of highly extensible polymers with strong HI (i.e., $z \gg 1$ and $\zeta_s/\zeta_c \gtrsim$

https://doi.org/10.1021/acs.macromol.4c01604
Macromolecules 2024, 57, 9668−9676

4.5), the elastic stress exerted on the thinning fluid filament becomes sufficient to influence the thinning dynamics during the early stages of polymer deformation. Accordingly, within the EC regime, the polymers behave as elastic Hookean springs (as per the Oldroyd-B model), continuing to stretch and accumulate strain toward near full extension when the filament breaks. Thus, the time scale at which elastic stresses become measurable approximately matches the longest relaxation time of the polymer, i.e., $\tau_{EC} \approx \tau$. In contrast, stiffer polymers with screened HI do not exert sufficient tension to modify the Newtonian-like thinning of the fluid filament until they are already significantly stretched. Consequently, stiffer polymers reach the EC regime in a significantly stretched state, behaving as nonlinear springs. This leads to a reduced EC regime and a time scale for measurable elastic stress $\tau_{EC} \ll \tau$. This also means that Wi_{EC} can reach a very high value $\gg 2/3$ within the EC regime (see the dependence of Wi_{EC} on $1/L$ shown in the inset of Figure 5d).

The criterion proposed by Campo-Deaño and Clasen[2] considering the elastic contribution of isolated (noninteracting) FENE chains is predictive of a lower concentration limit (c_{low}) above which the onset of polymer stretching (i.e., when the polymer behaves as a Hookean spring) generates sufficient stress to induce an EC regime. For flexible polymers, such as PS and PEO, $c_{low} < c^*$, indicating that even in the dilute case the polymer chains generate sufficient elastic stress to initiate the EC regime at the onset of stretching. For such flexible polymers having $c_{low} < c^*$ the consideration of isolated chains in the estimation of c_{low} holds and consistently $\tau \sim \tau_{EC}$. However, for relatively stiff polymers, such as λ-DNA, the predicted c_{low} falls well above c^* ($c_{low} > c^*$), violating the assumption of isolated polymer chains underlying the estimation of c_{low}. As such, c_{low} cannot be used as a concentration limit above which to expect $\tau \sim \tau_{EC}$. Indeed, for the λ-DNA at $c > c_{low}$, we still find $\tau_{EC} \ll \tau$. We also note that the estimation of c_{low} is not always simple because in most cases, Mw, τ_0, and L are not known *a priori* with sufficient accuracy to determine c_{low} reliably, especially for common polymer samples that are inherently polydisperse, presenting a large distribution of Mw, τ_0, and L. Additionally, these parameters are not straightforward to estimate because they rely on the correct choice of theory to adopt. In practice, the estimation of c_{low} is limited to certain model polymer and solvent systems.

CONCLUSION

In summary, capillary thinning extensional flow techniques are widely used and appealing due to their simplicity, minimal fluid volume requirements, and their provision of data to complement characterization by standard shear flow techniques. They also offer valuable insight into how a fluid responds to the self-selected uniaxial extensional flow that is generated in a thinning filament. However, we have shown that the longest relaxation time τ of a polymer cannot be universally retrieved by extracting a characteristic time τ_{EC} from the exponential filament decay in the EC regime of a capillary thinning experiment. This limitation stems from the polymer dynamics that occur during capillary thinning, which are not universal but strongly depend on the polymer extensibility. Our estimates indicate that for highly extensible macromolecules ($L \gtrsim 30$), the dynamics that occur during capillary thinning are in reasonable agreement with the predictions of models for which polymer orientation occurs primarily within the EC regime and which equate τ_{EC} with τ. However, for macromolecules of lower extensibility, it appears that significant orientation can occur prior to the onset of the EC regime. Consequently, the duration of the EC regime is reduced prior to the onset of finite extensibility effects, with the result that τ_{EC} is reduced relative to τ.

Previous research has highlighted inconsistencies between the characteristic time obtained from capillary thinning and that determined through traditional steady or oscillatory rheometric shear flow methods.[32,39,68,69] This has led to the concept that capillary thinning provides the "extensional relaxation time" of the polymer, a different time scale from the "shear relaxation time" retrieved from shear flow experiments. We acknowledge that the time scale for the onset of polymer orientation in shear and extension can be different and that this difference is yet to be fully understood.[50,70,71] However, our experiments, for the first time, compare capillary thinning measurements against another extensional flow (i.e., that in the OSCER device). Since the time scales obtained do not (in general) agree, the idea that capillary thinning yields the extensional relaxation time cannot be completely correct. In fact, based on our understanding, we would argue that τ_{EC} should not be thought of as a relaxation time but rather, perhaps, as an inverse strain rate beyond which elastic stresses become dominant in an extensional flow. We believe that τ_{EC} may in fact be a more appropriate metric than τ to describe the elastic nature of the fluid under extensional flows, which is not necessarily captured by τ (i.e., for relatively stiff and inelastic polymers with large τ but small τ_{EC}). On the other hand, when the polymer extensibility is low ($L \lesssim 30$), "relaxation time" measurements made by capillary thinning techniques should be interpreted carefully as they most likely do not accurately describe the orientational dynamics of the polymer.

This work highlights the need to develop experimental systems to properly measure the orientational dynamics of macromolecules during filament thinning, which are currently either inferred from simulations or estimated by applying significant simplifying assumptions to experimental thinning data. Such dynamical measurements may aid in the development of microstructural models and analytical expressions for the extrapolation of the true material properties of diverse complex fluids.

MATERIALS AND METHODS

The specifics of the commercially available polymers are reported in Table S1. For each polymer, we report the weight-averaged Mw provided by the supplier from which the contour length l_c is estimated. For the CMC sample, the Mw reported in Table S1 is obtained from the weight-averaged degree of polymerization (N = 2540) estimated from intrinsic viscosity measurements and the measured degree of substitution (specified in ref. 71). For the double-stranded ct-DNA and λ-DNA, the weight-averaged number of base pairs (bp) was measured by using a Femto Pulse System (Agilent Technologies).

Neutral Polymers. For PS, the contour length is computed as $l_c = nl$, where n is the number of bonds and l = 0.154 nm is the C−C bond length. The mean-squared end-to-end length at equilibrium is computed as $\langle R^2 \rangle = C_\infty n l^2$ with the Flory's characteristic ratio C_∞ = 9.7. The length of a Kuhn segment is given as $b = \langle R^2 \rangle / l_c$ = 1.5 nm.[63] For poly(ethylene oxide) (PEO), the contour length is estimated as $l_c = (\mathrm{Mw}/\mathrm{M_{mon}}) l_{mon}$ using the monomer molecular weight $\mathrm{M_{mon}}$ = 44 g/mol and the monomer size

https://doi.org/10.1021/acs.macromol.4c01604
Macromolecules 2024, 57, 9668−9676

l_{mon} = 0.278 nm. The mean-squared end-to-end length at equilibrium is computed as $\langle R^2 \rangle = 6R_g^2$, by knowing the dependence of the radius of gyration R_g as a function of Mw retrieved from scattering experiments, R_g = 0.02 $Mw^{0.58}$.[72]

Polyelectrolytes. For the polyelectrolytes HA and CMC, the contour length is estimated as $l_c = (Mw/M_{mon})l_{mon}$. For HA, M_{mon} = 400 g/mol and l_{mon} = 0.95 nm, while for CMC M_{mon} = 231 g/mol and l_{mon} = 0.95 nm. For the DNA solutions, l_c is estimated by multiplying the number of bp with the average separation distance (0.34 nm).[73] For HA, HA_{NaCl}, and CMC, the persistence length, l_p, is estimated as described previously.[71] The persistence length l_p is described as $l_p = l_{p0} + l_{pE}$, where l_{p0} is the intrinsic contribution to the total persistence length and l_{pE} is the electrostatic contribution.[74] The electrostatic persistence length, l_{pE}, is estimated as $l_{pE} \approx \xi/2$, where ξ is the correlation length or mesh size. The dependence of ξ vs the polyelectrolyte concentration (c) is extracted from scattering data (Figure 2 in Lopez et al.[75] and Figure 6 in Salamon et al.[76]). For HA and CMC, we provide in Table S1 the relation of l_{pE} as a function of c (mg/mL) and l_{p0} values from literature. At 1.5 M NaCl, we expect screening of electrostatic interactions, thus for HA_{NaCl} we use l_{pE} = 0 nm. The l_p for the DNA samples is extracted from literature (Figure 4 in Brunet et al.).[77] For polyelectrolytes, the mean-squared end-to-end length at equilibrium is computed using a worm-like chain model as $\langle R^2 \rangle = 2l_p l_c - 2l_p^2(1 - \exp(-l_c/l_p))$ and the length of a Kuhn segment is computed as $b = 2l_p$.[63] The DNA concentrations were measured using a UV−vis spectrophotometer (Nanodrop, Thermo Fisher) by measuring absorbance at a wavelength of 260 nm and using an extinction coefficient of 0.020 (mL μg^{-1} cm^{-1}). The λ-DNA at c = 660 μg/mL was prepared by concentrating the stock solution (at $c \approx$ 300 μg/mL) by centrifugation (4000g) using Amicon ultra centrifugal filters with a 100 kDa molecular weight cutoff.

Measurements. The characteristic dimensions of the OSCER device are the width of the channel arm W and the height H, with an aspect ratio $H/W \geq 10$ to generate a good approximation to a two-dimensional flow. OSCER devices with a range of widths ($0.1 \leq W \leq 0.3$ mm) and heights ($2 \leq H \leq 3$ mm) were fabricated in fused silica glass by selective laser-induced etching to achieve the required extension rates to detect birefringence while minimizing inertia.[78] The Reynolds number at the onset of detectable birefringence is $Re = \rho Q/(\eta H) < 0.1$ with ρ the fluid density, Q the volumetric flow rate within the device (controlled by syringe pumps, Nemesys, Cetoni) and η the shear viscosity at a nominal shear rate of $Q/(W^2H)$. The steady-state birefringence is measured with the OSCER device on an upright microscope and using a Photron Crysta PI-1P high-speed polarization imaging camera. The SRM[2] is implemented on a commercial capillary breakup extensional rheometer (CaBER 1, Thermo Haake) fitted with end plates of diameter D_p = 6 mm, and imaging is performed using a Phantom Miro 310 high-speed camera. Filament diameter analysis is performed using a MATLAB routine as specified in ref. 66, following the guidelines given in ref. 79

■ ASSOCIATED CONTENT

Supporting Information

The Supporting Information is available free of charge at https://pubs.acs.org/doi/10.1021/acs.macromol.4c01604.

This includes specifications of the polymer samples, notes on the effect of plate diameter on the SRM experiment and data for λ-DNA at $c > c_{low}$ in the SRM experiment (PDF)

■ AUTHOR INFORMATION

Corresponding Authors

Vincenzo Calabrese − *Micro/Bio/Nanofluidics Unit, Okinawa Institute of Science and Technology Graduate University, Onna-son, Okinawa 904-0495, Japan;* orcid.org/0000-0001-5974-9217; Email: vincenzo.calabrese@oist.jp

Simon J. Haward − *Micro/Bio/Nanofluidics Unit, Okinawa Institute of Science and Technology Graduate University, Onna-son, Okinawa 904-0495, Japan;* orcid.org/0000-0002-1884-4100; Email: simon.haward@oist.jp

Author

Amy Q. Shen − *Micro/Bio/Nanofluidics Unit, Okinawa Institute of Science and Technology Graduate University, Onna-son, Okinawa 904-0495, Japan;* orcid.org/0000-0002-1222-6264

Complete contact information is available at: https://pubs.acs.org/10.1021/acs.macromol.4c01604

Notes

The authors declare no competing financial interest.

■ ACKNOWLEDGMENTS

The authors gratefully acknowledge the support of Okinawa Institute of Science and Technology Graduate University with subsidy funding from the Cabinet Office, Government of Japan. V.C., S.J.H., also acknowledge the financial support from the Japanese Society for the Promotion of Science (JSPS, Grant Nos. 24K07332, 24K17736, and 24K00810). The authors thank Prof. Christian Clasen (KU Leuven) for feedback on the original manuscript and Fabian Hillebrand (Micro/Bio/Nanofluidics Unit, OIST) for the stimulating discussions. An earlier version of this manuscript was previously made available on arXiv with DOI: 10.48550/arXiv.2403.04103.

■ REFERENCES

(1) Anna, S. L.; McKinley, G. H. Elasto-capillary thinning and breakup of model elastic liquids. *J. Rheol.* **2001**, *45*, 115−138.

(2) Campo-Deaño, L.; Clasen, C. The slow retraction method (SRM) for the determination of ultra-short relaxation times in capillary breakup extensional rheometry experiments. *J. Non-Newtonian Fluid Mech.* **2010**, *165*, 1688−1699.

(3) Nelson, W. C.; Kavehpour, H. P.; Kim, C. J. A miniature capillary breakup extensional rheometer by electrostatically assisted generation of liquid filaments. *Lab Chip* **2011**, *11*, 2424−2431.

(4) Bhattacharjee, P. K.; McDonnell, A. G.; Prabhakar, R.; Yeo, L. Y.; Friend, J. Extensional flow of low-viscosity fluids in capillary bridges formed by pulsed surface acoustic wave jetting. *New J. Phys.* **2011**, *13*, 023005.

(5) Dinic, J.; Zhang, Y.; Jimenez, L. N.; Sharma, V. Extensional relaxation times of dilute, aqueous polymer solutions. *ACS Macro Lett.* **2015**, *4*, 804−808.

(6) Keshavarz, B.; Sharma, V.; Houze, E. C.; Koerner, M. R.; Moore, J. R.; Cotts, P. M.; Threlfall-Holmes, P.; McKinley, G. H. Studying the effects of elongational properties on atomization of weakly viscoelastic solutions using Rayleigh Ohnesorge Jetting Extensional Rheometry (ROJER). *J. Non-Newtonian Fluid Mech.* **2015**, *222*, 171−189.

(7) Sharma, V.; Haward, S. J.; Serdy, J.; Keshavarz, B.; Soderlund, A.; Threlfall-Holmes, P.; McKinley, G. H. The rheology of aqueous solutions of ethyl hydroxy-ethyl cellulose (EHEC) and its hydrophobically modified analogue (hmEHEC): Extensional flow response in capillary break-up, jetting (ROJER) and in a cross-slot extensional rheometer. *Soft Matter* **2015**, *11*, 3251−3270.

(8) Mathues, W.; Formenti, S.; McIlroy, C.; Harlen, O. G.; Clasen, C. CaBER vs ROJER−Different time scales for the thinning of a weakly elastic jet. *J. Rheol.* **2018**, *62*, 1135−1153.

(9) Rajesh, S.; Thiévenaz, V.; Sauret, A. Transition to the viscoelastic regime in the thinning of polymer solutions. *Soft Matter* **2022**, *18*, 3147−3156.

(10) Gaillard, A.; Herrada, M. A.; Deblais, A.; Eggers, J.; Bonn, D. Beware of CaBER: Filament thinning rheometry does not always give 'the'relaxation time of polymer solutions. *Phys. Rev. Fluids* **2024**, *9*, 073302.
(11) Vadillo, D. C.; Mathues, W.; Clasen, C. Microsecond relaxation processes in shear and extensional flows of weakly elastic polymer solutions. *Rheol. Acta* **2012**, *51*, 755−769.
(12) Papageorgiou, D. T. On the breakup of viscous liquid threads. *Phys. Fluids* **1995**, *7*, 1529−1544.
(13) McKinley, G. H.; Tripathi, A. How to extract the Newtonian viscosity from capillary breakup measurements in a filament rheometer. *J. Rheol.* **2000**, *44*, 653−670.
(14) Bazilevsky, A. V.; Entov, V. M.; Rozhkov, A. N. *Third European Rheology Conference and Golden Jubilee Meeting of the British Society of Rheology*; Oliver, D. R. ed.; Springer: Dordrecht, 1990; pp. 4143
(15) Entov, V. M.; Hinch, E. J. Effect of a spectrum of relaxation times on the capillary thinning of a filament of elastic liquid. *J. Non-Newtonian Fluid Mech* **1997**, *72*, 31−54.
(16) Clasen, C.; Plog, J.; Kulicke, W.-M.; Owens, M.; Macosko, C.; Scriven, L.; Verani, M.; McKinley, G. H. How dilute are dilute solutions in extensional flows? *J. Rheol.* **2006**, *50*, 849−881.
(17) Stelter, M.; Brenn, G.; Yarin, A.; Singh, R.; Durst, F. Validation and application of a novel elongational device for polymer solutions. *J. Rheol.* **2000**, *44*, 595−616.
(18) Stelter, M.; Brenn, G.; Yarin, A.; Singh, R.; Durst, F. Investigation of the elongational behavior of polymer solutions by means of an elongational rheometer. *J. Rheol.* **2002**, *46*, 507−527.
(19) Gier, S.; Wagner, C. Visualization of the flow profile inside a thinning filament during capillary breakup of a polymer solution via particle image velocimetry and particle tracking velocimetry. *Phys. Fluids* **2012**, *24*, 053102.
(20) De Gennes, P. G. Coil-stretch transition of dilute flexible polymers under ultrahigh velocity gradients. *J. Chem. Phys.* **1974**, *60*, 5030−5042.
(21) Hinch, E. J. Mechanical models of dilute polymer solutions in strong flows. *Phys. Fluids* **1977**, *20*, S22−S30.
(22) Larson, R. G.; Magda, J. J. Coil-stretch transitions in mixed shear and extensional flows of dilute polymer solutions. *Macromolecules* **1989**, *22*, 3004−3010.
(23) Perkins, T. T.; Smith, D. E.; Chu, S. Single polymer dynamics in an elongational flow. *Science* **1997**, *276*, 2016−2021.
(24) Wagner, C.; Bourouiba, L.; McKinley, G. H. An analytic solution for capillary thinning and breakup of FENE-P fluids. *J. Non-Newtonian Fluid Mech.* **2015**, *218*, 53−61.
(25) McKinley, G. H. *Visco-elasto-capillary thinning and break-up of complex fluids*, Massachusetts Institute of technology, 2005.
(26) Miller, E.; Clasen, C.; Rothstein, J. P. The effect of step-stretch parameters on capillary breakup extensional rheology (CaBER) measurements. *Rheol. Acta* **2009**, *48*, 625−639.
(27) Dinic, J.; Sharma, V. Macromolecular relaxation, strain, and extensibility determine elastocapillary thinning and extensional viscosity of polymer solutions. *Proc. Natl. Acad. Sci. U. S. A.* **2019**, *116*, 8766−8744.
(28) Liang, R. F.; Mackley, M. R. Rheological characterization of the time and strain dependence for polyisobutylene solutions. *J. Non-Newtonian Fluid Mech.* **1994**, *52*, 387−405.
(29) Plog, J. P.; Kulicke, W.-M.; Clasen, C. Influence of the molar mass distribution on the elongational behaviour of polymer solutions in capillary breakup. *Appl. Rheol.* **2005**, *15*, 28−37.
(30) Duxenneuner, M. R.; Fischer, P.; Windhab, E. J.; Cooper-White, J. J. Extensional properties of hydroxypropyl ether guar gum solutions. *Biomacromolecules* **2008**, *9*, 2989−2996.
(31) Haward, S. J.; Sharma, V.; Butts, C. P.; McKinley, G. H.; Rahatekar, S. S. Shear and extensional rheology of cellulose/ionic liquid solutions. *Biomacromolecules* **2012**, *13*, 1688−1699.
(32) Jimenez, L. N.; Dinic, J.; Parsi, N.; Sharma, V. Extensional relaxation time, pinch-off dynamics, and printability of semidilute polyelectrolyte solutions. *Macromolecules* **2018**, *51*, 5191−5208.
(33) Walter, A. V.; Jimenez, L. N.; Dinic, J.; Sharma, V.; Erk, K. A. Effect of salt valency and concentration on shear and extensional rheology of aqueous polyelectrolyte solutions for enhanced oil recovery. *Rheol. Acta* **2019**, *58*, 145−157.
(34) Rosello, M.; Sur, S.; Barbet, B.; Rothstein, J. P. Dripping-onto-substrate capillary breakup extensional rheometry of low-viscosity printing inks. *J. Non-Newtonian Fluid Mech.* **2019**, *266*, 160−170.
(35) Jimenez, L. N.; Martínez Narváez, C. D. V.; Sharma, V. Capillary breakup and extensional rheology response of food thickener cellulose gum (NaCMC) in salt-free and excess salt solutions. *Phys. Fluids* **2020**, *32*, 012113.
(36) Martínez Narváez, C. D. V.; Mazur, T.; Sharma, V. Dynamics and extensional rheology of polymer-surfactant association complexes. *Soft Matter* **2021**, *17*, 6116−6126.
(37) Lauser, K. T.; Rueter, A. L.; Calabrese, M. A. Small-volume extensional rheology of concentrated protein and protein-excipient solutions. *Soft Matter* **2021**, *17*, 9624−9635.
(38) Jimenez, L. N.; Martínez Narváez, C. D. V.; Sharma, V. Solvent properties influence the rheology and pinching dynamics of polyelectrolyte solutions: Thickening the pot with glycerol and cellulose gum. *Macromolecules* **2022**, *55*, 8117−8132.
(39) Zhang, D. Y.; Calabrese, M. A. Temperature-controlled dripping-onto-substrate (DoS) extensional rheometry of polymer micelle solutions. *Soft Matter* **2022**, *18*, 3993−4008.
(40) Soetrisno, D. D.; Martínez Narváez, C. D. V.; Sharma, V.; Conrad, J. C. Concentration regimes for extensional relaxation times of unentangled polymer solutions. *Macromolecules* **2023**, *56*, 4919−4928.
(41) Morozova, S.; Schmidt, P. W.; Metaxas, A.; Bates, F. S.; Lodge, T. P.; Dutcher, C. S. Extensional flow behavior of methylcellulose solutions containing fibrils. *ACS Macro Lett.* **2018**, *7*, 347−352.
(42) Latinwo, F.; Schroeder, C. M. Model systems for single molecule polymer dynamics. *Soft Matter* **2011**, *7*, 7907−7913.
(43) Schroeder, C. M.; Babcock, H. P.; Shaqfeh, E. S. G.; Chu, S. Observation of polymer conformation hysteresis in extensional flow. *Science* **2003**, *301*, 1515−1519.
(44) Schroeder, C. M. Single polymer dynamics for molecular rheology. *J. Rheol.* **2018**, *62*, 371−403.
(45) Smith, D. E.; Chu, S. Response of flexible polymers to a sudden elongation flow. *Science* **1998**, *281*, 1335−1340.
(46) Hsiao, K.-W.; Dinic, J.; Ren, Y.; Sharma, V.; Schroeder, C. M. Passive non-linear microrheology for determining extensional viscosity. *Phys. Fluids* **2017**, *29*, 121603.
(47) Haward, S. J.; Oliveira, M. S. N.; Alves, M. A.; McKinley, G. H. Optimized cross-slot geometry for microfluidic extensional rheometry. *Phys. Rev. Lett.* **2012**, *109*, 128301.
(48) Haward, S. J.; McKinley, G. H.; Shen, A. Q. Elastic instabilities in planar elongational flow of monodisperse polymer solutions. *Sci. Rep.* **2016**, *6*, 33029.
(49) Zhou, Y.; Schroeder, C. M. Dynamically heterogeneous relaxation of entangled polymer chains. *Phys. Rev. Lett.* **2018**, *120*, 267801.
(50) Smith, D. E.; Babcock, H. P.; Chu, S. Single-polymer dynamics in steady shear flow. *Science* **1999**, *283*, 1724−1727.
(51) Teixeira, R. E.; Babcock, H. P.; Shaqfeh, E. S.; Chu, S. Shear thinning and tumbling dynamics of single polymers in the flow-gradient plane. *Macromolecules* **2005**, *38*, 581−592.
(52) Shrewsbury, P. J.; Muller, S. J.; Liepmann, D. Effect of flow on complex biological macromolecules in microfluidic devices. *Biomed. Microdevices* **2001**, *3*, 225−238.
(53) Liu, Y.; Jun, Y.; Steinberg, V. Longest relaxation times of double-stranded and single-stranded DNA. *Macromolecules* **2007**, *40*, 2172−2176.
(54) Juarez, G.; Arratia, P. E. Extensional rheology of DNA suspensions in microfluidic devices. *Soft Matter* **2011**, *7*, 9444−9452.
(55) Pan, S.; At Nguyen, D.; Sridhar, T.; Sunthar, P.; Ravi Prakash, J. Universal solvent quality crossover of the zero shear rate viscosity of semidilute DNA solutions. *J. Rheol.* **2014**, *58*, 339−368.

https://doi.org/10.1021/acs.macromol.4c01604
Macromolecules 2024, 57, 9668−9676

(56) Colby, R. H. Fiber spinning from polymer solutions. *J. Rheol.* **2023**, *67*, 1251−1255.
(57) Calabrese, V.; Shen, A. Q.; Haward, S. J. Effects of polydispersity and concentration on elastocapillary thinning of dilute polymer solutions. *arXiv* **2024**.
(58) Zinelis, K.; Abadie, T.; McKinley, G. H.; Matar, O. K. The fluid dynamics of a viscoelastic fluid dripping onto a substrate. *arXiv* **2024**.
(59) Doi, M.; Edwards, S. F. *The Theory of Polymer Dynamics*; Oxford University Press: New York, 1988.
(60) Lang, C.; Kohlbrecher, J.; Porcar, L.; Radulescu, A.; Sellinghoff, K.; Dhont, J. K. G.; Lettinga, M. P. Microstructural understanding of the length- and stiffness-dependent shear thinning in semidilute colloidal rods. *Macromolecules* **2019**, *52*, 9604−9612.
(61) Calabrese, V.; Haward, S. J.; Shen, A. Q. Effects of shearing and extensional flows on the alignment of colloidal rods. *Macromolecules* **2021**, *54*, 4176−4185.
(62) Tsentalovich, D. E.; Ma, A. W.; Lee, J. A.; Behabtu, N.; Bengio, E. A.; Choi, A.; Hao, J.; Luo, Y.; Headrick, R. J.; Green, M. J. Relationship of extensional viscosity and liquid crystalline transition to length distribution in carbon nanotube solutions. *Macromolecules* **2016**, *49*, 681−689.
(63) Rubinstein, M.; Colby, R. H. *Polymer Physics*; Oxford University Press: New York, 2003.
(64) Lundahl, M. J.; Berta, M.; Ago, M.; Stading, M.; Rojas, O. J. Shear and extensional rheology of aqueous suspensions of cellulose nanofibrils for biopolymer-assisted filament spinning. *Eur. Polym. J.* **2018**, *109*, 367−378.
(65) Lang, C.; Hendricks, J.; Zhang, Z.; Reddy, N. K.; Rothstein, J. P.; Lettinga, M. P.; Vermant, J.; Clasen, C. Effects of particle stiffness on the extensional rheology of model rod-like nanoparticle suspensions. *Soft Matter* **2019**, *15*, 833−841.
(66) Calabrese, V.; Gyorgy, C.; Haward, S. J.; Neal, T. J.; Armes, S. P.; Shen, A. Q. Microstructural dynamics and rheology of worm-like diblock copolymer nanoparticle dispersions under a simple shear and a planar extensional flow. *Macromolecules* **2022**, *55*, 10031−10042.
(67) Hsieh, C.-C.; Larson, R. G. Prediction of coil-stretch hysteresis for dilute polystyrene molecules in extensional flow. *J. Rheol.* **2005**, *49*, 1081−1089.
(68) Arnolds, O.; Buggisch, H.; Sachsenheimer, D.; Willenbacher, N. Capillary breakup extensional rheometry (CaBER) on semi-dilute and concentrated polyethyleneoxide (PEO) solutions. *Rheol. Acta* **2010**, *49*, 1207−1217.
(69) Sachsenheimer, D.; Hochstein, B.; Willenbacher, N. Experimental study on the capillary thinning of entangled polymer solutions. *Rheol. Acta* **2014**, *53*, 725−739.
(70) Hur, J. S.; Shaqfeh, E. S.; Babcock, H. P.; Chu, S. Dynamics and configurational fluctuations of single DNA molecules in linear mixed flows. *Phys. Rev. E* **2002**, *66*, 011915.
(71) Calabrese, V.; Porto Santos, T.; Lopez, C. G.; Lettinga, M. P.; Haward, S. J.; Shen, A. Q. Extensibility governs the flow-induced alignment of polymers and rod-like colloids. *Phys. Rev. Res.* **2024**, *6*, L012042.
(72) Devanand, K.; Selser, J. Asymptotic behavior and long-range interactions in aqueous solutions of poly (ethylene oxide). *Macromolecules* **1991**, *24*, 5943−5947.
(73) Reisner, W.; Pedersen, J. N.; Austin, R. H. DNA confinement in nanochannels: physics and biological applications. *Rep. Prog. Phys.* **2012**, *75*, 106601.
(74) Dobrynin, A. V.; Rubinstein, M. Theory of polyelectrolytes in solutions and at surfaces. *Prog. Polym. Sci.* **2005**, *30*, 1049−1118.
(75) Lopez, C. G.; Colby, R. H.; Cabral, J. T. Electrostatic and hydrophobic interactions in NaCMC aqueous solutions: Effect of degree of substitution. *Macromolecules* **2018**, *51*, 3165−3175.
(76) Salamon, K.; Aumiler, D.; Pabst, G.; Vuletic, T. Probing the mesh formed by the semirigid polyelectrolytes. *Macromolecules* **2013**, *46*, 1107−1118.
(77) Brunet, A.; Tardin, C.; Salomé, L.; Rousseau, P.; Destainville, N.; Manghi, M. Dependence of DNA persistence length on ionic strength of solutions with monovalent and divalent salts: a joint theory−experiment study. *Biophys. J.* **2016**, *110*, 403a.
(78) Burshtein, N.; Chan, S. T.; Toda-Peters, K.; Shen, A. Q.; Haward, S. J. 3D-printed glass microfluidics for fluid dynamics and rheology. *Curr. Opin. Colloid Interface Sci.* **2019**, *43*, 1−14.
(79) Ng, H. C.; Poole, R. J. Highlighting the need for high-speed imaging in capillary breakup extensional rheometry. *Meas. Sci. Technol.* **2021**, *32*, 095301.

https://doi.org/10.1021/acs.macromol.4c01604
Macromolecules 2024, 57, 9668−9676